AD-A076 499 BINARY SYSTEMS INC SILVER SPRING MD F/G 20/4
WAVENUMBER SPECTRAL MEASUREMENT OF TURBULENT BOUNDARY LAYER WAL--ETC(U)
APR 79 P S TONG N00014-72-C-0318
UNCLASSIFIED WBR-79-2 NL

| OF |
AD
A076499

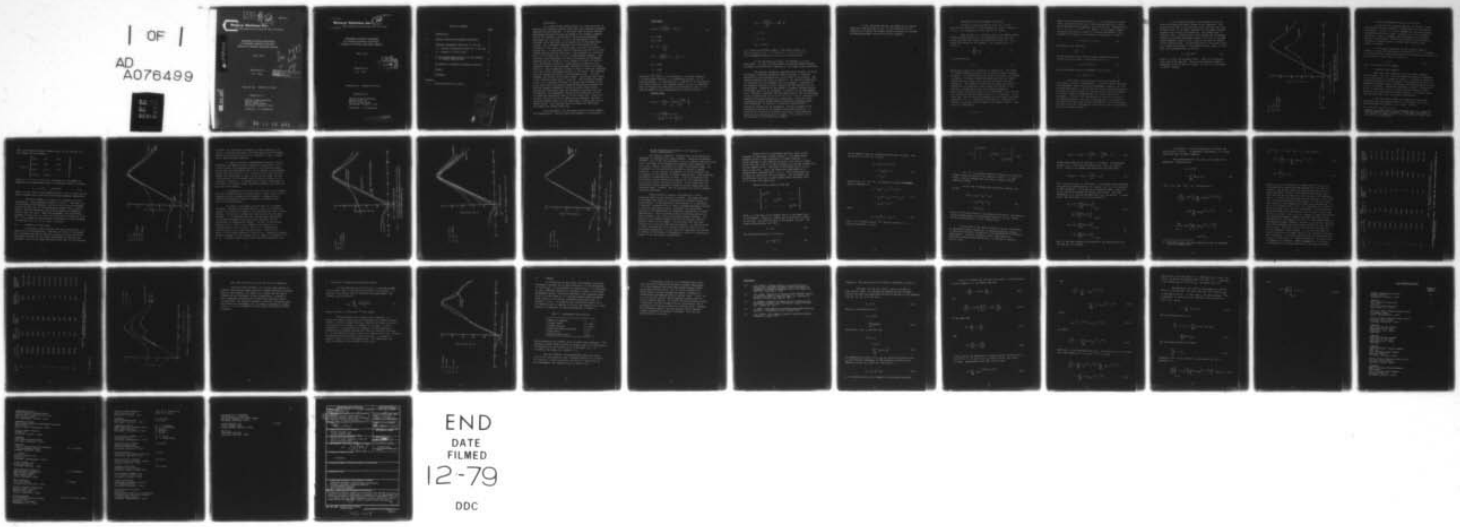

END
DATE
FILMED
12-79
DDC

LEVEL IV

WBR-79-2

Binary Systems Inc.

10750 Columbia Pike, Silver Spring, Md. 20901 (301) 593-2960

AD A076499

WAVENUMBER SPECTRAL MEASUREMENT OF TURBULENT BOUNDARY LAYER WALL PRESSURE BY MAXIMUM LIKELIHOOD METHODS

April 1979

See 1473 or back page

Submitted by:

P.S. Tong

This document has been approved for public release and sale; its distribution is unlimited.

Contract No.: N00014-72-C-0318

Submitted to:

Office of Naval Research
Section Code 713
800 N. Quincy Street
Arlington, Virginia 22217

Attention: H. Fitzpatrick

DDC FILE COPY

79 11 13 231

WBR-79-2

Binary Systems Inc.

10750 Columbia Pike, Silver Spring, Md. 20901 (301) 593-2960

WAVENUMBER SPECTRAL MEASUREMENT OF TURBULENT BOUNDARY LAYER WALL PRESSURE BY MAXIMUM LIKELIHOOD METHODS

April 1979

DDC
RECEIVED
NOV 14 1979
E

Submitted by:

P.S. Tong

Contract No.: N00014-72-C-0318

Submitted to:

Office of Naval Research
Section Code 713
800 N. Quincy Street
Arlington, Virginia 22217

Attention: H. Fitzpatrick

This document has been approved for public release and sale; its distribution is unlimited.

TABLE OF CONTENTS

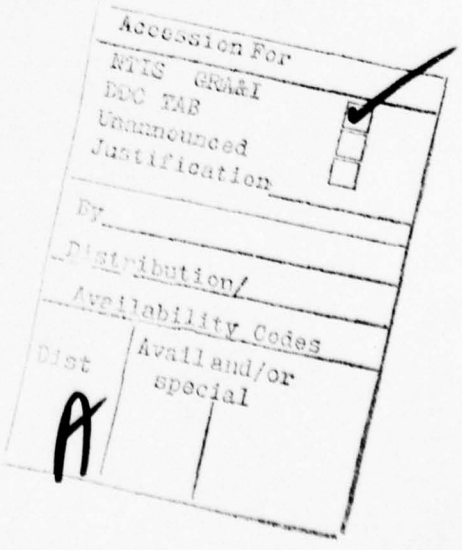

1. Introduction

In a recent Binary Systems report [1], the difficulty of measuring the turbulent bounary layer (TBL) wall-pressure wavenumber spectrum has been detailed. It was shown that to achieve desired measurement accuracy, the gain and phase of the acoustic elements must be very carefully controlled if conventional measurement techniques are to be used. In fact, the requirements are so stringent as to cast doubt on the feasibility of the measurement program. For subsequent comparison with the technique to be proposed in this report, we repeat some of the earlier designed figures here. It was shown that the required array has 40 1.2-inch elements butting against each other. The tolerance is 0.058 dB in gain, 0.3° in phase, and 1.73 mil in phase-center location. Even with such tight tolerances, the array can measure the wavenumber spectrum only for values of $(k/2\pi)$ between -4.0 and +4.0 cycle/ft with 3-dB accuracy at 100 Hz. These results are based on the assumption that the TBL wavenumber spectrum is given by the Chase model [2]. Such a spectrum is shown in Figure 1 where the frequency is 100 Hz and the free-stream velocity is 25 ft/sec. This spectrum does not include the effect of finite element width. For thin elements, the effect will be small anyway. Notice the power levels at the convection peak and at 0 cycle/ft. The difference exceeds 55 dB. It is extremely difficult to control the sidelobes of the array factor using conventional spectral measurement technique so that the leakage everywhere is below the actual signal level. Although the Chase model does not necessarily represent the true TBL spectrum, the measurement technique to be used must be able to handle the eventuality that it is the correct one. Since it is the more difficult of the two models being suggested, the other being the Gardner model [3], the Chase model is being used as the design target. Any technique which can handle the Chase model will handle the Gardner model also.

For convenience, the functional forms of the two models are repeated here. They are taken from Appendix A of Reference [1].

Chase Model

$$P_o(k,\omega) = \frac{c_t \rho^2 v_*^3}{a} K^2 K_t^{-5} \qquad (1)$$

$$c_t = 0.063$$

$$v_* = 0.04U$$

$$K^2 = k^2 + \frac{1}{12a^2}$$

$$K_t^2 = \frac{\omega - U_c k}{h\, v_*} + \frac{1}{\Delta^2} + k^2$$

$$U_c = 0.68U$$

$$\Delta = 1.08a$$

$$h = 3.7$$

Throughout this report, k is wavenumber; ω is angular frequency; U is free-stream velocity; U_c is convection velocity; 'a' is cylinder radius; ρ is fluid density (2 slug/ft^3 in our discussion); v_* is shear velocity. The spectral density $P_o(k,\omega)$ is defined so that its integral over both positive and negative K and ω is the expected square of the circumferentially averaged pressure.

Gardner Model

$$P_o(k,\omega) = \frac{\phi(\omega)}{8\pi^2} \left[\frac{1 - e^{-\pi \alpha_2 N_s}}{\pi\ \alpha_2\ N_s} \right] G \qquad (2)$$

$$G = \frac{2\alpha_1 N_s}{\left(\alpha_1 N_s \frac{U}{U_c}\right)^2 + \left(ka - \frac{U}{U_c} N_s\right)^2}$$

$$\phi(\omega) = \frac{2\rho^2 v_*^3}{N_s^2} \left(\frac{v^*}{U}\right) a^2$$

$$\alpha_1 = 0.1$$

$$\alpha_2 = 1.7$$

$$N_s = (\omega a/U)$$

N_s is called the Strouhal number. Each model presents the spectral density $P_o(k, \omega)$ in terms of ρ, U, and a; a set of fixed numerical parameters; and a function of N_s and ka.

In the discussion to follow the emphasis is on the Chase model. As seen, the Chase model is much more sharply peaked and hence, more difficult to measure for the reason given previously.

The spectral estimation technique being proposed is called the maximum likelihood estimation (MLE) technique. A detailed derivation of this technique will not be given in this report. The relevant equations are given in Section 2. An intuitive explanation of the merits of this procedure will be attempted. In Section 3, the inherent potential of MLE to measure the TBL spectrum will be investigated. Tradeoffs of the number of elements, element spacing, and element size will be discussed. In Section 4, the measurement error induced by imperfect gain and phase control will be considered. It will be shown that the MLE technique alone is still inadequate for measuring the Chase spectrum but a combination of MLE and a more conventional Barlett window spectral estimation technique seems quite promising. In Section 5, a practical implementation problem of the MLE will be considered. The MLE is based on the correlation function of the random process being measured. In practice this function is obtained from time or space averaging which will not be perfect but the effect of the imperfection on the estimation will be shown to be small.

In the concluding section, we summarize the results which have been obtained so far. We also speculate on the possibility of making the element spacing nonuniform to achieve the same measurement accuracy with fewer elements.

2. Maximum-Likelihood Wavenumber Estimation

The MLE is first proposed by Capon [4] in 1969. A more concise discussion of this technique is given by Lacoss [5] in 1971. Our discussion is more akin to the latter.

Suppose there is a receiving array of N equally spaced elements whose outputs are to be combined linearly into one single sum such that certain objectives are fulfilled. Let x_i denote the outputs of the elements. The combined sum z is given by

$$z = \sum_{i=1}^{N} a_i x_i^* \tag{3}$$

In vector notation,

$$z = \underline{a}\ \underline{x}^\dagger \tag{4}$$

where both $\underline{a}$ and $\underline{x}$ are row vectors of dimension N. The symbol '*' denotes complex conjugate and '†' denotes complex conjugate transpose. In conventional array design, the vector $\underline{a}$ introduces a sequence of delays or phase rotations such that the element outputs due to a signal from a desired direction will add coherently. The undesired 'noise' from all other directions is controlled by an amplitude taper across the aperture at the expense of reduced array gain and increased beamwidth. Specifically, the design does not take advantage of any information concerning the environment even if it is available. On the other hand, the MLE technique measures the environment and takes advantage of it. It obtains the environmental information by forming a correlation matrix based on the element outputs. This matrix R is defined by

$$R = E[\underline{x}^\dagger\ x] \tag{5}$$

where E[x] is the expected value of x. It then derives a weight vector $\underline{a}$ which holds the gain in the desired direction to unity and minimizes the power from all other directions. Mathematically, if $S = (1, e^{jk\Delta}, \ldots, e^{j(N-1)k\Delta})$, where Δ is the element spacing, represents the steering vector of a desired wavenumber k, this procedure of finding $\underline{a}$ is equivalent to minimizing σ^2 given by

$$\sigma^2 = E[\underline{z}\ \underline{z}^\dagger] = \underline{a}\ R\ \underline{a}^\dagger \qquad (6)$$

subjected to the constraint

$$\underline{a}S^\dagger = 1$$

The optimization can be achieved using Lagrange multipliers. Without going into detail, the solution of $\underline{a}$ is

$$\underline{a} = S^*\ R^{-1}/SR^{-1}S^\dagger \qquad (8)$$

and the estimated power at wavenumber k is given by

$$P_L = (SR^{-1}\ S^\dagger)^{-1} \qquad (9)$$

Intuitively, the MLE would be superior because the environment is usually inhomogeneous. As in the case of TBL noise, the disturbance coming from certain wavenumber region(s) is often stronger than others. A better receiving array should obviously be configured in such a manner so that the nulls of the array should be placed in those wavenumbers where the interference is the strongest. In fact, if an interference is close to one side of the desired direction, the peak of the beam should be pointed to the other side with a null on the interference. In such an event, the signal gain will decrease but the overall signal-to-interference ratio will actually improve.

In the formulation above, the assumption that the receiving elements be equally spaced is not important. Any spacing can be used as long as their exact locations are known. As shown later, it is rather important to know these locations precisely for the MLE to be effective. Any random error in location, gain, or phase control could degrade the performance seriously in certain wavenumber regions. In order to overcome these drawbacks, there will be a need to use the more conventional technique also. As explained earlier, the weight vector $\underline{a}$ is chosen on the basis of the steering vector alone. In this case, the estimated power is given by

$$P_C = \frac{1}{N^2} (SRS^{\dagger}) \qquad (10)$$

where S is again the steering vector. There is no amplitude taper across the aperture. This uniform weighting scheme is sometimes called the Barlett window. In (10), N is the number of sensor elements.

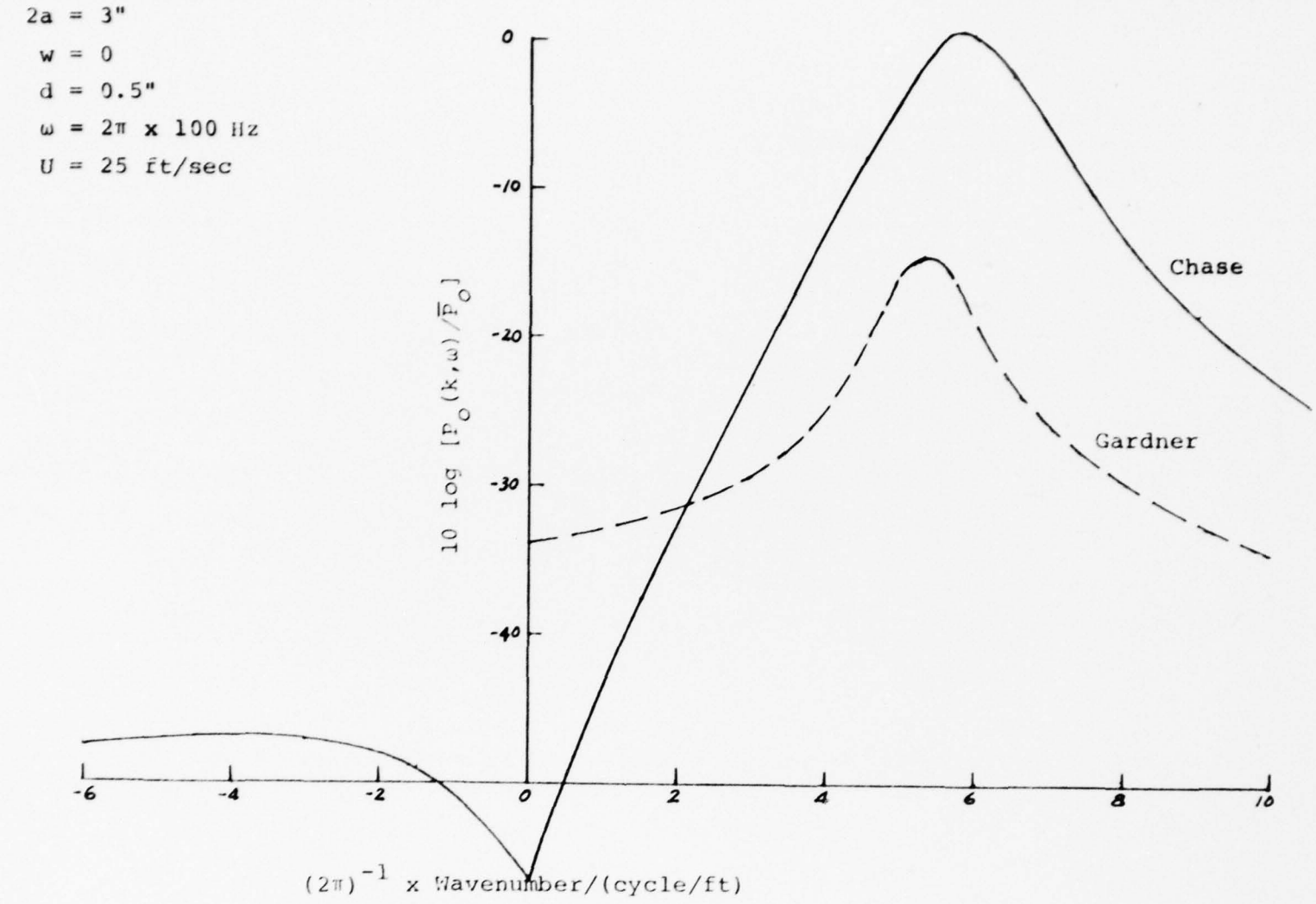

Figure 1. Chase and Gardner Models of TBL Wall-Pressure Spectrum (Normalized to the Peak of the Chase Model, $\bar{P}_o$)

3. Inherent Measurement Capability of the MLE

In this section, the applicability of the MLE to this measurement program is explored. Imperfections in the elements are ignored. In fact, it will be assumed that the exact spatial correlation matrix R is known. Although it is not a necessary condition, it will be assumed that the elements are uniformly spaced. In particular, we shall investigate the performance as functions of element spacing, element width, and the total number of elements.

In all cases considered, the TBL random process is assumed to follow the Chase model as given by Eq. (1). If elements of finite width are used, the spectrum will be modified by a $\sin(x)/(x)$ multiplicative factor where x is given by

$$x = wk/2 \qquad (11)$$

and w is the width of the element.

3.1 Infinitely Thin Elements

The first case considered deal with sensor elements without width, i.e., w=0. The ideal Chase TBL spectrum normalized to its peak level $\bar{P}_o$, is shown in Figure 1. In order to study the inherent capability of the ML method, the correlation matrix R is obtained by inverse Fourier transforming the Chase spectrum as given by Eq. (1) directly. Numerical techniques are used. The span for $(k/2\pi)$ is taken from -24 to +24 cycle/ft* which should be wide enough to avoid any spectral foldover problem. A 512-point transform has been used in all the Fourier computations.

Since the random process is assumed to be spatially stationary, the correlation function is a function only of the spacing between the elements, i.e., R(m,n) = R(m-n).

---

* Actually the upper limit of the wavenumber span is 2π times the inverse element spacing selected. In most cases considered in this report, the spacing is 0.5 inch. Therefore the upper limit on $(k/2\pi)$ is 24 cycle/foot.

Thus, the correlation matrix needed in Eq. (9) is given by (m,n are indices of the elements)

$$R_{(m,n)} = \begin{bmatrix} r(0) & r(1) & r(2) \ldots \\ r(-1) & r(0) & r(1) \ldots \\ r(-2) & r(-1) & r(0) \ldots \\ r(-N+1) & r(-N+2) & \ldots \end{bmatrix} \qquad (12)$$

where $r(i,j) = r(i-j) = E[x_i\ x_j^*]$ and where N is the number of elements in the measurement array. The steering vector is given by

$$S = (1,\ e^{jk\Delta},\ldots,\ e^{j(N-1)k\Delta}) \qquad (13)$$

where j is $\sqrt{-1}$ and Δ is the element spacing. Eqs. (9) and (10) are used to compute the ML and the conventional estimates respectively.

The first example is an array of 25 elements with 0.5-inch spacing. The estimates are shown in Figure 2. The dash line is the original ideal spectrum, the solid line is the ML estimate and the dot-dash line is the conventional estimate with a Barlett window. Near the convection peak both estimates are reasonably close to the true value. Near zero wavenumber, the conventional estimate of log $P_o(k,\omega)$ is 30 dB off while the ML estimate is 12 dB off. If we impose a 3-dB criterion of performance, the ML estimate is acceptable only for $(k/2\pi)$ above 1 cycle/ft.

3.2 Elements of Finite Width

In practice, sensor elements must have finite width. Its effect will be considered here. Besides, the width of the element will introduce some spatial smoothing capability which effectively suppresses the power of the higher wavenumbers and improves the estimates. Most of the cases considered below use 0.5-inch elements.

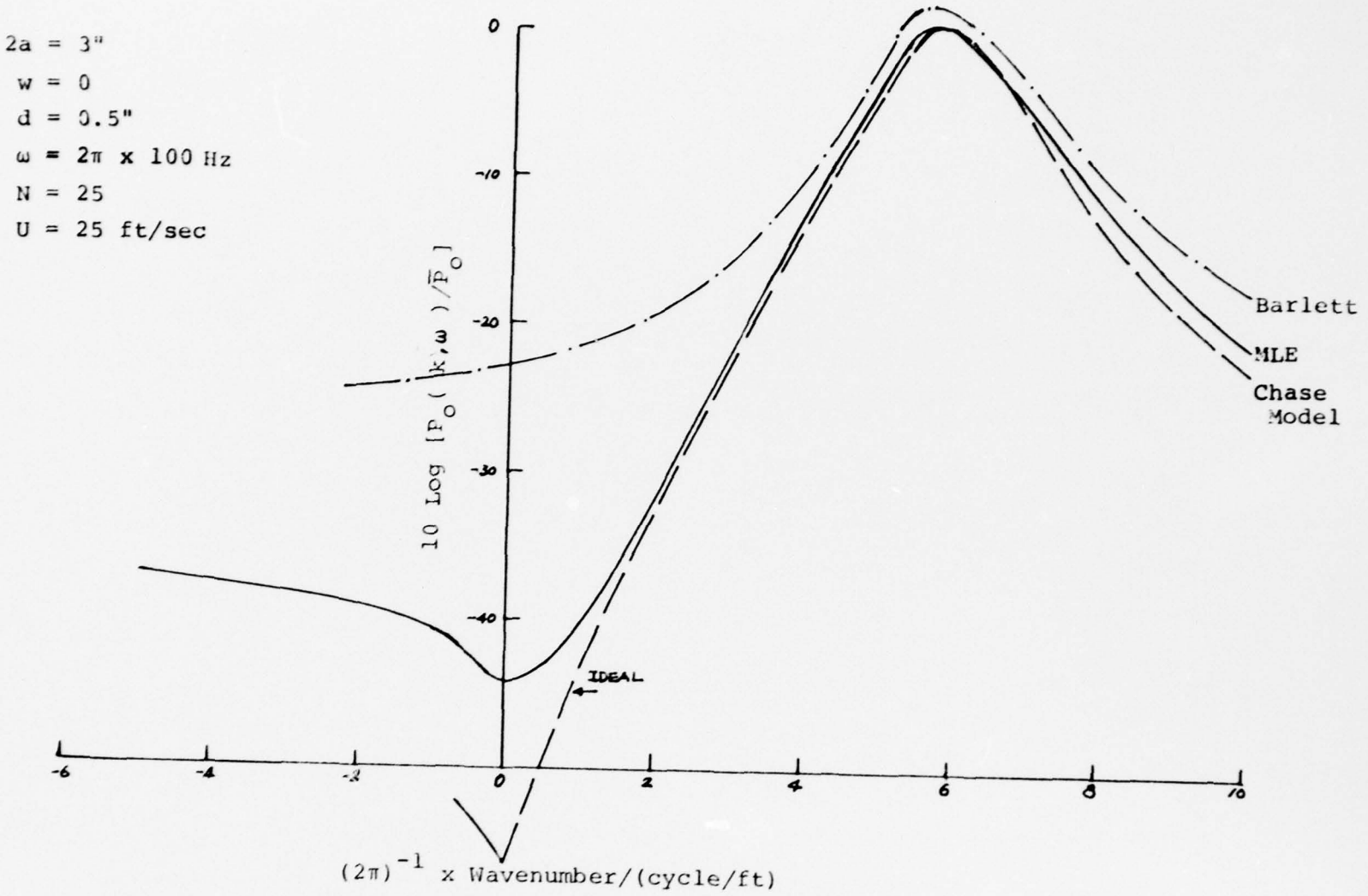

Figure 2. Estimates of the Chase Model, $w = 0$; Normalized to the True Peak in the Chase Model, $\bar{P}_o$

For them, the first cutoff frequency of these elements is at $\pm$24 Hz. As stated previously, the Chase spectrum at the element output will be modified by a sin x/x function. Figure 3 shows such a modified Chase spectrum.

In order to provide a comprehensive picture of the ML estimates, the number of array elements is varied from 5 to 25. Figure 4 shows the estimated spectra of five different arrays. Notice that the improvement from 5 to 10 elements is considerably larger than that from 20 to 25. In fact, even at the zero wavenumber, the improvement is only 2 dB in the last case. By the 3-dB cirterion, the 25-element array is good for values of $k/2\pi$ to about 0.5 cycle/ft. It appears that to obtain an estimate no more than 3 dB from the actual spectrum everywhere the array size may have to be doubled.

As compared with the array with infinitely thin elements, the finite element array is actually better. This is due to the averaging effect provided by the elements. Perhaps one can improve performance by further increasing the element width. This is investigated next.

In Figure 5, MLE spectra for an array of 25 elements are shown. The width is changed from 0.5 inch to 0.62 and 0.74 inches. The dotted line shown is the ideal spectrum with 0.5-inch elements. We have not included the ideal spectra for the wider elements. It is observed that there is some minor improvement in the zero-wavenumber region with wider elements, but the improvement is progressively smaller. In fact, the difference between 0.62 in. and 0.74 in. elements is too small to be distinguishable in this figure. Thus, it is concluded that element width is not a very critical factor. There will be about 1 dB difference between 0.5 and 0.74 in. Subsequent analysis actually assumes 0.5-inch elements and the number of elements is set at 25. A somewhat shorter array would have been acceptable also.

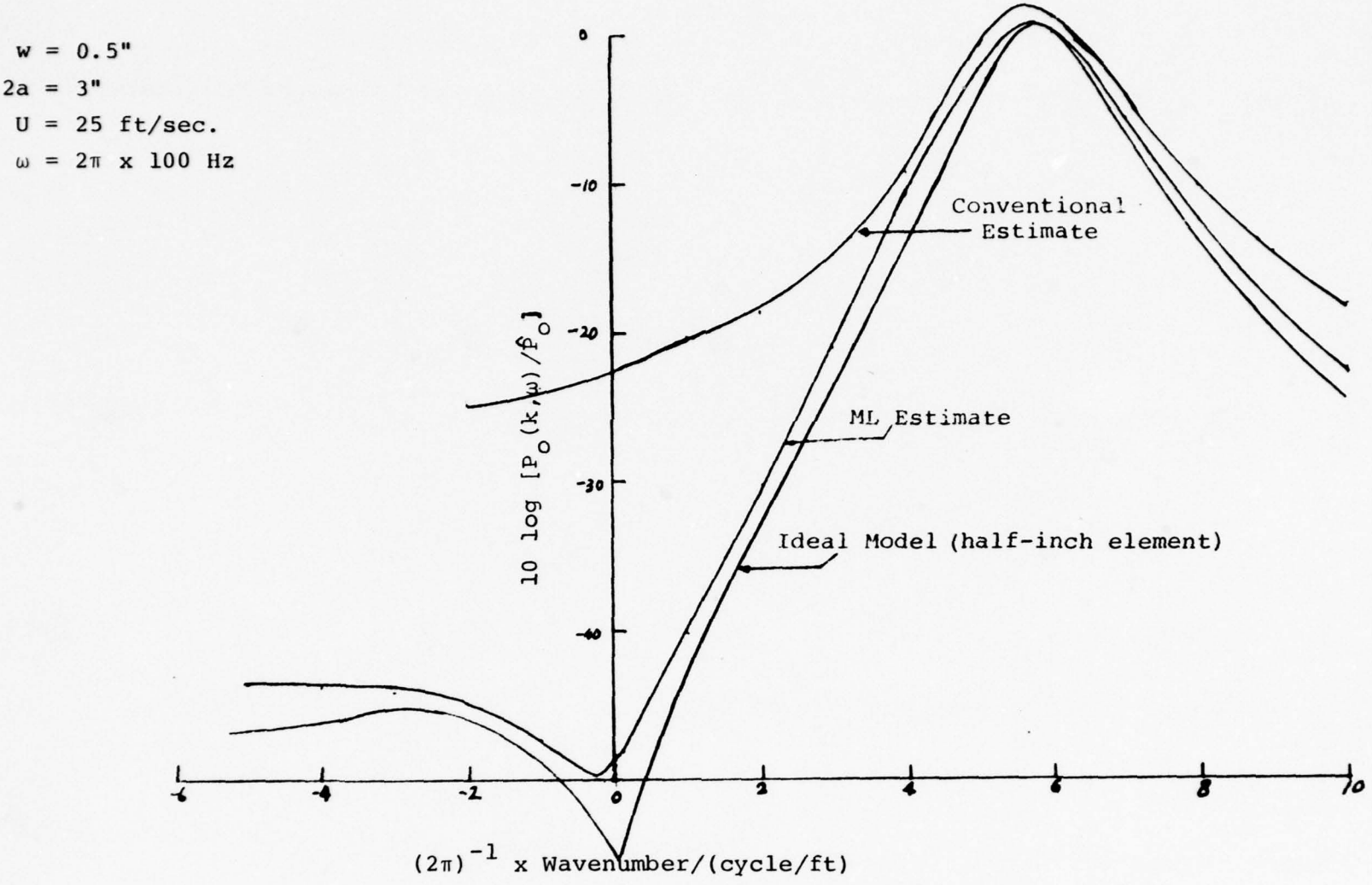

Figure 3. Flow-Noise Spectra, 25 Elements, 0.5-Inch Spacing, 0.5-Inch Element Width, Normalized to the Peak of the Ideal Chase Spectrum, $\hat{P}_o$

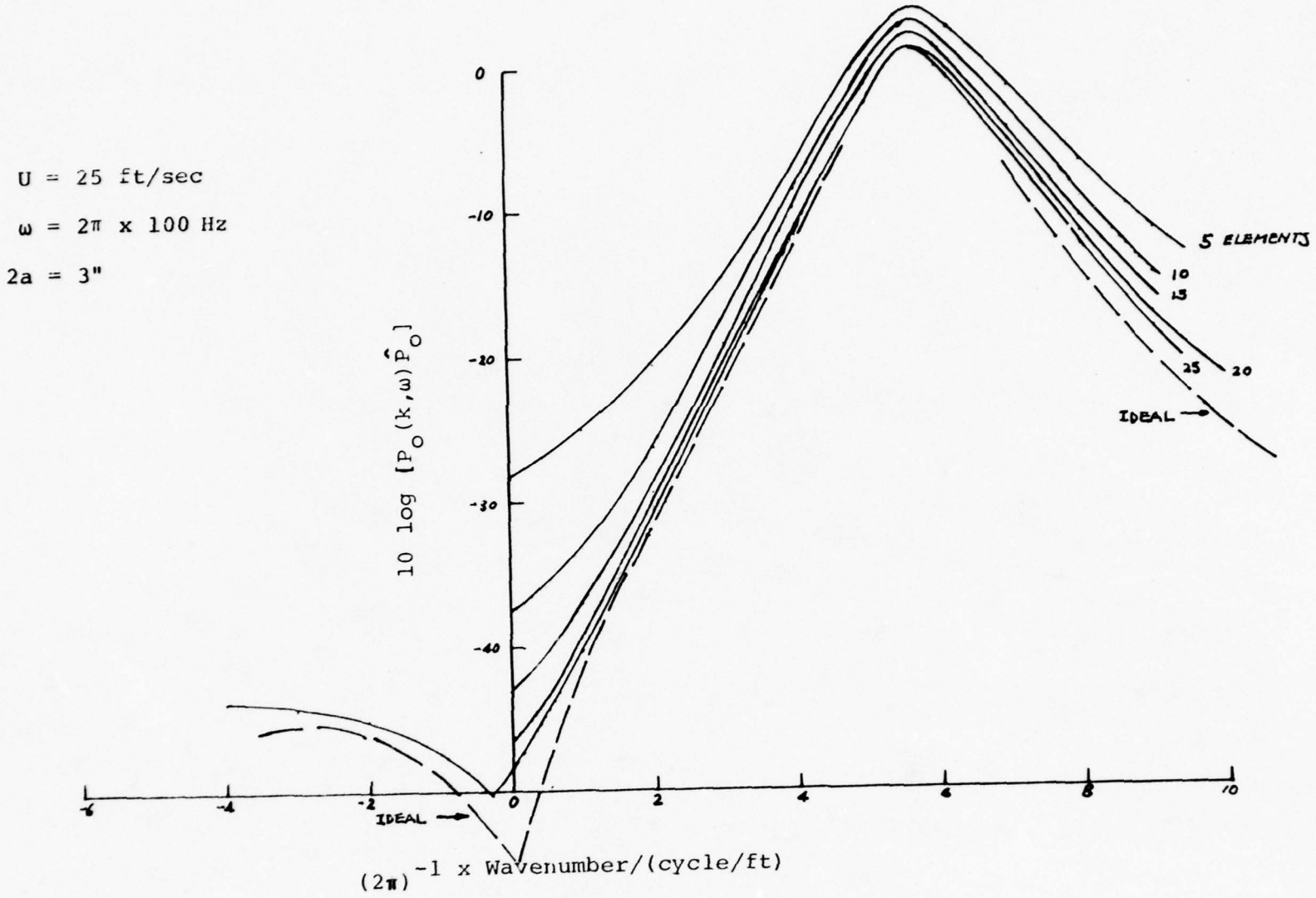

Figure 4. ML Estimates, w = 0.5", d = 0.5".

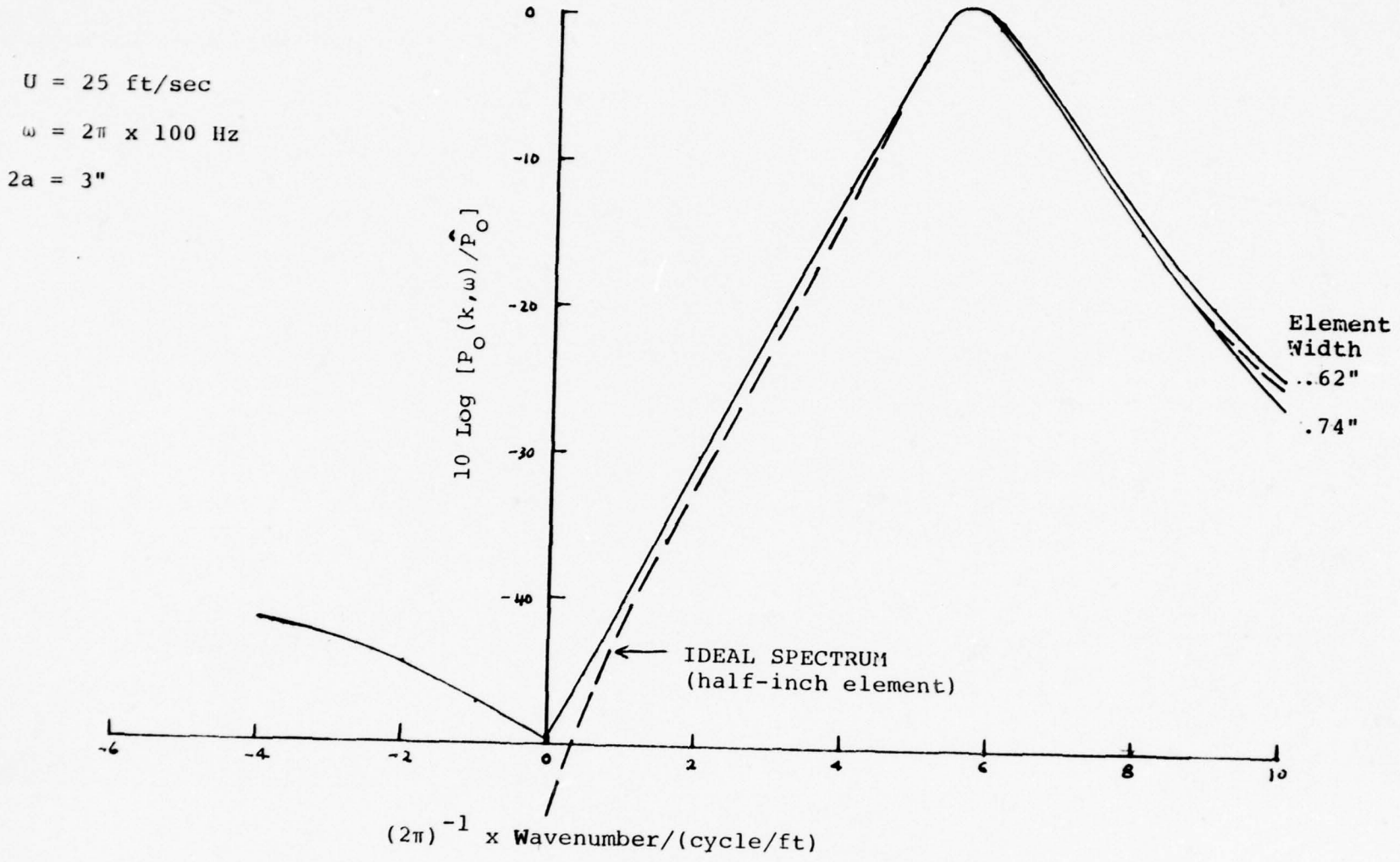

Figure 5. ML Estimates, w=d, 25 Elements.

4. ML and Conventional Estimates in the Presence of Sensor Imperfections

The result in Section 3 indicates that the ML estimation technique is acceptable with ideal elements. Although the spectral-estimate error at the zero-wavenumber region is greater than the desired limit, the shape of the spectrum is reasonably well preserved. If it is only a matter of choosing the Chase or the Gardner model, the ML estimate will be sufficiently accurate to effect a logical selection. In this section, the behavior of the ML estimator will be analyzed in the presence of element imperfections. Both analytical and empirical techniques will be used. It will be shown that the ML estimate is quite sensitive to errors near the convection peak but is quite stable near the null region. On the other hand, the conventional Barlett estimate is shown to be more stable near the convection peak. Together, the two estimates will provide adequate estimates everywhere.

Sensor errors are usually unavoidable but in many situations they are not difficult to handle. The common procedure to overcome these errors is to calibrate the sensors by means of known signals. In the case being investigated, it is impossible to generate a pressure field of known frequency-wavenumber spectrum to test the experimental array. Therefore, the measurement technique to be adopted must be reasonably insensitive to element imperfections. There are three kinds of errors associated with a sensor element: gain, phase, and element-center placement. The centroid of an element's sensitivity may not coincide with the physical center of the element. Any deviation from the ideal location will affect the estimator performance. If each deviation is known, compensation can of course be made and there will be negligible degradations. If the individual deviations are unknown, an estimate of the degree of degradation in terms of a statistical measure of the deviations is appropriate.

Observe that in a narrowband analysis, delay or displacement is equivalent to phase rotation. An element-center placement error is thus equivalent to a phase rotation. A signal component of the form exp [j(kz-ωt)] will yield an output of the form exp [j(kd-ωt)] from an element at d and exp [j(kd+kδ-ωt)] from an element at d+δ. The ratio of the second output to the first is exp [jkδ]. Thus, the phase error equivalent to an element-center placement error δ is kδ. This relationship will be useful in specifying the array design. For the moment this relationship allows us to treat element-center placement error as if it were just phase error.

Define an error matrix T such that

$$T = \begin{bmatrix} \alpha_1 e^{-j\theta_1} & 0 & 0 \ldots \\ 0 & \alpha_2 e^{-j\theta_2} & 0 \ldots \\ 0 & \ldots\ldots & \alpha_N e^{-j\theta_N} \end{bmatrix}$$

where α_n is the gain of the element and θ_n is the phase error of the element. Ideally, α_n should all be unity and θ_n should all be zero. Let $\underline{x}$ be the input in the absence of error. The actual received output will be $\underline{y}$;

$$\underline{y} = \underline{x}\,T \tag{14}$$

The correlation matrix R_y is given by

$$R_y = E[\underline{y}^T\,\underline{y}^*] \tag{15}$$

We are assuming that all random processes have zero mean. Substituting (14) into (15), we have

$$R_y = E[(\underline{x}\,T)^T\,(\underline{x}\,T)^*]$$

$$= T^T\,E[\underline{x}^T\,\underline{x}^*]\,T^* \qquad (16)$$

$$= T^T\,R_x\,T^*$$

Substituting (16) into (9), the maximum likelihood **wavenumber** spectral estimate is

$$P_L = (S_x(T^T\,R_x\,T^*)^{-1}\,S_x^\dagger)^{-1}$$

$$= (S_x(T^T)^{-1}\,R_x^{-1}\,T^{*-1}\,S_x^\dagger)^{-1} \qquad (17)$$

$$= (S_y\,R_x^{-1}\,S_y^\dagger)^{-1}$$

where

$$S_y = S_x(T^T)^{-1} = S_x\,T^{-1} \qquad (18)$$

Since T is a diagonal matrix, $T^T=T$ and the inverse of T is readily obtainable. In fact,

$$T^{-1} = \begin{bmatrix} \alpha_1^{-1} e^{+j\theta_1} & 0 & 0 \ldots \\ 0 & \alpha_2^{-1} e^{+j\theta_2} & 0 \ldots \\ 0 & 0 & \alpha_N^{-1} e^{j\theta_N} \end{bmatrix} \qquad (19)$$

Eq. (17) is important because it permits us to consider element errors as errors in the steering vector S. In other words, it may be assumed that the array is perfect but the steering is wrong.

In the case of conventional estimates, from Eq. (10), we have

$$\begin{aligned} (N^2) P_c &= S_x (T^T R_x T^*) S_x^\dagger \\ &= S_x T^T R_x T^* S_x^\dagger \\ &= S_z R_x S_z^\dagger \end{aligned} \qquad (20)$$

Again, we can treat errors in the elements as errors in the steering vector although there is a difference between S_y and S_z, namely, the error matrices are T^{-1} and T respectively.

On the basis of the above discussion, we have transformed an imperfect-element problem into an imperfect-steering problem. If the errors are small, deviations in the estimates can be obtained analytically. To do so, we employ a well known theorem in functional analysis which states that if a function is analytic near x_o, then

$$f(x_o+\delta) = f(x_o) + \frac{f'(x_o)}{1!}\,\delta + \frac{f''(x_o)}{2!}\,\delta^2 + \ldots \qquad (21)$$

Higher order terms can be ignored if δ is small. In the present context, x is either gain or phase error. f(x) is either P_L or P_c. Since it is assumed that the errors have mean zero,

$$E[f(x_0+\delta) - f(x_0)] = \frac{f''(x)}{2!}\,E\{\delta^2] \qquad (22)$$

$E[\delta^2]$ is the variance of the errors. In the case being considered the quantities represented by f(x), namely P_L or P_c, are functions of many variables. If the errors are basically small, there will be no interaction between the various error terms. The total degradation is a linearly weighted sum of all the errors. In other words, the deviations in P_L or P_c are given by

$$\Delta P_L = \tfrac{1}{2}\,\sigma_\beta{}^2\left[\sum_n \partial^2 P_L/\partial\beta_n{}^2\right]_{\beta_n=1} + \tfrac{1}{2}\sigma_\theta{}^2\left[\sum_n \partial^2 P_L/\partial\theta_n{}^2\right]_{\theta_n=\theta_n} \qquad (23)$$

$$\Delta P_c = \tfrac{1}{2}\,\sigma_\beta{}^2\left[\sum_n \partial^2 P_c/\partial\beta_n{}^2\right]_{\beta_n=1} + \tfrac{1}{2}\,\sigma_\theta{}^2\left[\sum_i \partial^2 P_c/\partial\theta_n{}^2\right]_{\theta_n=\theta_n} \qquad (24)$$

where it has been assumed the variances of the sensor errors are the same for all elements.

In practice, it is more convenient to consider the ratio $\Delta P_L/P_L$ or $\Delta P_c/P_c$. In subsequent discussions, it is these quantities that are being computed.

The differentiation of P_L and P_c is carried out in Appendix A. Defining Q by

$$Q = S\, R^{-1} S^{\dagger}$$

$$= \sum_{n,m} b_{nm}\, s_n\, s_m^{*} \tag{25}$$

$\partial^2 P_L / \partial \theta_\ell^{\,2}$ and $\partial^2 P_L / \partial \beta_\ell^{\,2}$ are given by **

$$\frac{\partial^2 P_L}{\partial \theta_\ell^{\,2}} = 2Q^{-3} \left[-2 \sum_{n \neq \ell} \mathrm{Im}\left(b_{\ell n} e^{j\theta_\ell}\, e^{-j\theta_n}\right) \right]^2$$

$$+ 2Q^{-2} \sum_{n \neq \ell} \mathrm{Re}\left(b_{\ell n} e^{j\theta_\ell}\, e^{-j\theta_n}\right) \tag{26}$$

$$\frac{\partial^2 P_L}{\partial \beta_\ell^{\,2}} = 2Q^{-3} \left[2 \sum_{n} \mathrm{Re}\left(b_{\ell n} e^{j\theta_\ell}\, e^{-j\theta_n}\right) \right]^2$$

$$-2Q^{-2}\, b_{\ell\ell} \tag{27}$$

** The notation Re(x) and Im(x) denote the real and imaginary part of x respectively.

and $\partial^2 P_c / \partial \theta_\ell^{\,2}$ and $\partial^2 P_c / \partial \beta_\ell^{\,2}$ are given by

$$(N^2)\ \frac{\partial^2 P_c}{\partial \theta_\ell^{\,2}} = -2 \sum_{n \neq \ell} \mathrm{Re}(r_{\ell n} e^{j\theta_\ell} e^{-j\theta_n}) \tag{28}$$

$$(N^2)\ \frac{\partial^2 P_c}{\partial \theta_\ell^{\,2}} = 2\, r'_{\ell\ell} \tag{29}$$

where r_{nm} are the elements of R rather than R^{-1} as in (25). Substituting the appropriate derivatives into (23) and (24), we obtain the desired analytical expression relating gain or phase (placement) errors to the spectral measurement error. Note that the derivatives are to be evaluated at the desired β_n and θ_n. We shall term these derivatives appearing in (23) and (24), the error-sensitivity coefficients. If they are large, small errors in the elements will cause large degradations. In Eq. (26) we observed that $\partial^2 P_L / \partial \theta_\ell^{\,2}$ is dependent on Q^{-3} and Q^{-2}, which are equal to $P_L^{\,3}$ and $P_L^{\,2}$. Therefore, it is obvious that the error-sensitivity coefficients will be large in the region where P_L is large. Table 1a,b is a summary of these coefficients for various wavenumbers assuming the Chase spectrum is being measured with a 25-element array with 0.5-inch elements and 0.5-inch spacing between elements. As seen P_L is the least sensitive near zero wavenumber and 10,000 times as sensitive near the convection peak. The sense of error is such that the peak level will be reduced by large amounts. P_c, on the other hand, is fairly insensitive to element errors in all regions of interest but, relatively, it is least sensitive near the convection peak. Figure 6 is the result of a sample simulation. The phase error is assumed to be Gaussian. When we compare this to Figure 6, it confirms the conclusions obtained by the analytical means.

$\frac{k}{2\pi}$ ft^{-1}	10 log $(P_o(k,\omega)/\hat{P}_o)$	Phase Sensitivity, $\partial^2 P_c/\partial\theta^2$	Acceptable Phase Error*	Amplitude Sensitivity, $\partial^2 P_c/\partial\beta^2$	Acceptable Amplitude Range*
0	-91.69	1.6	$>10^o$	-.16	$.8<\beta<1.2$
1	-83.42	-0.32	$>10^o$	-2.1	$.8<\beta<1.2$
2	-73.45	-22	9.2^o	-23.7	$.85<\beta<1.14$
3	-64.55	-193	3.1^o	-194.8	$.94<\beta<1.06$
4	-54.91	-1716	1.1^o	-1718.2	$.98<\beta<1.02$
5	-45.77	-14069	$.4^o$	-14070	$.994<\beta<1.006$
6	-43.32	-24793	$.3^o$	-24789	$.995<\beta<1.005$
7	-49.17	-6443	$.5^o$	-6448	$.99<\beta<1.01$
8	-55.85	-1381	1.2^o	-1384	$.98<\beta<1.02$
9	-61.41	-383	2.2^o	-385	$.97<\beta<1.03$
10	-65.97	-133	3.8^o	-134	$.94<\beta<1.06$

Table 1a. MLE Sensitivity Coefficients
25 Elements, d = 0.5", w = 0.5", $\omega=2\pi$x100 Hz

* The analysis assumes small errors. An error less than 3-dB in the spectral estimation is deemed acceptable.

$\frac{k}{2\pi}$ ft^{-1}	10 log $(P_o(k,\omega)/P_o)$	Phase Sensitivity, $\partial^2 P_c/\partial\theta^2$	Acceptable Phase Error*	Amplitude Sensitivity, $\partial^2 P_c/\partial\beta^2$	Acceptable Amplitude Range*
0	-66.08	43.2	4^o	45.2	$0.91<\beta<1.09$
1	-64.52	29.5	9^o	31.5	$.88<\beta<1.12$
2	-62.14	16.2	$>10^o$	18.2	$.8<\beta<1.2$
3	-58.19	53.3	$>10^o$	7.3	$.8<\beta<1.2$
4	-51.75	-33.2	$>10^o$	1.7	$.8<\beta<1.2$
5	-44.18	- 1.7	$>10^o$	.3	$.8<\beta<1.2$
6	-42.28	- 1.8	$>10^o$	.2	$.8<\beta<1.2$
7	-47.47	- 1.4	$>10^o$	.6	$.8<\beta<1.2$
8	-53.51	0.5	$>10^o$	2.5	$.8<\beta<1.2$
9	-58.12	5.2	$>10^o$	7.2	$.8<\beta<1.2$
10	-61.46	13.6	$>10^o$	15.5	$.8<\beta<1.2$

Figure 1b. Convention Estimate Sensitivity Coefficients, 25 elements, d = w = 0.5", $\omega=2\pi$x100 Hz

* See Table 1a.

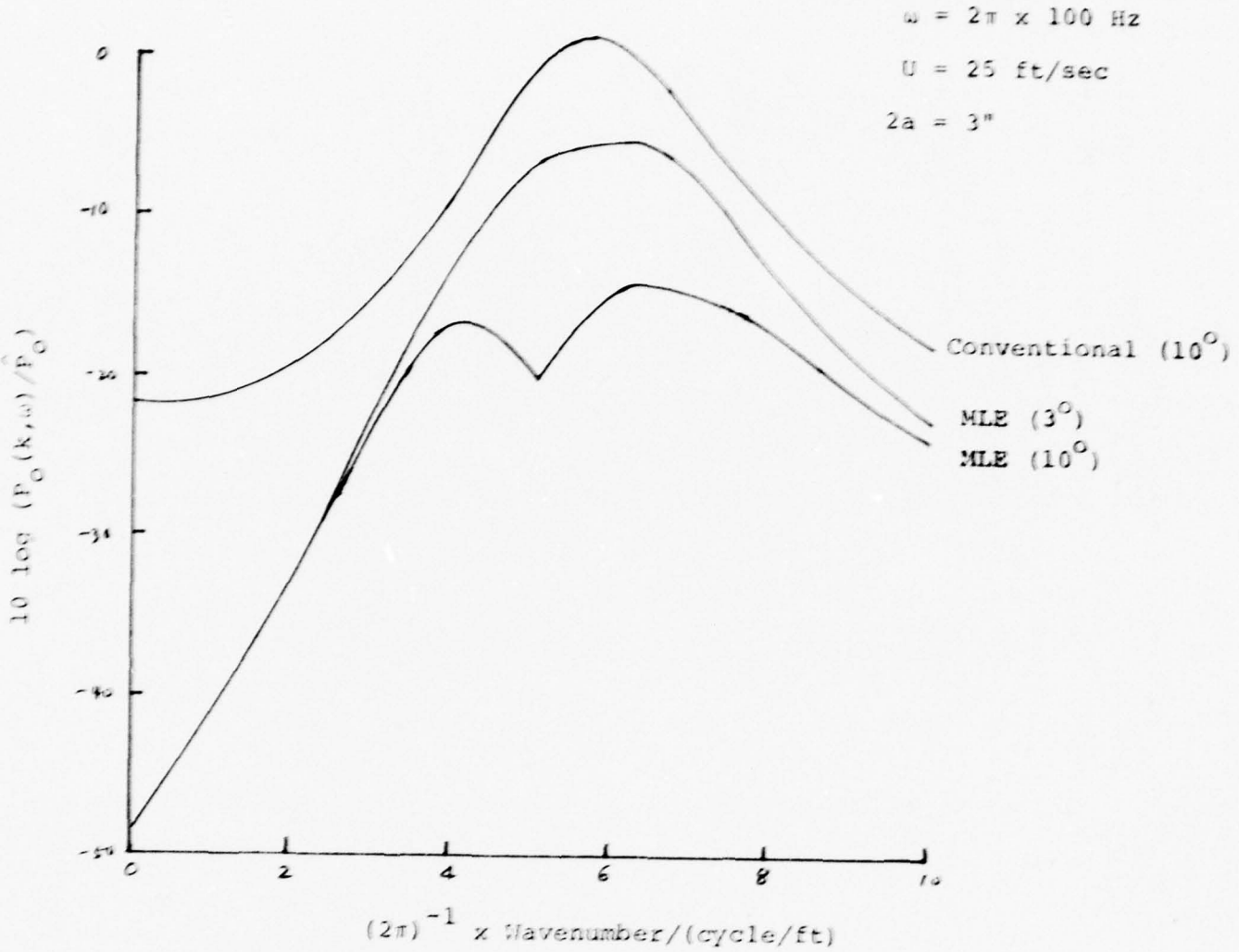

Figure 6. Spectral Estimate with Sensor Errors, 25 elements, ω = 0.5 inch.

Note that the errors in (23) and (24) are additive.

From this error analysis, it is clear that relying on maximum likelihood estimate alone will impose unrealistic requirements on the sensors. But there is no reason why one cannot combine the two estimates, ML and conventional, to obtain a very respectable estimate with a much more practical design. In particular, the combined estimate around the convection peak and around zero wavenumber will be almost unaffected by sensor errors. In the intermediate regions, some interpolation seems desirable.

5. The Effect of Imperfect Correlation Function

In the discussion up to this point, it has been assumed that an exact copy of the correlation matrix R is available. In practice, this matrix must be obtained from measurements. The elements r_{nm} are given by

$$r_{nm} = \sum_{i=1}^{M} \frac{x_n(i)x_m^*(i)}{M} \tag{30}$$

where the index i denotes the i^{th} time sample.

How large must M be to obtain good estimates? An analytical answer is believed to be obtainable but rather difficult. However, it can be shown relatively simply that M must be greater than N which is the number of elements in the array. If this constraint is not satisfied, the inversion process required in computing P_L is unstable because the rank of R would be less than N. In the simulations done to date, M is usually set at N+5. Results obtained are quite consistent and satisfactory. An example is shown in Figure 7 for a 25-element array. For comparison, the ideal ML estimate is also shown in dotted line.

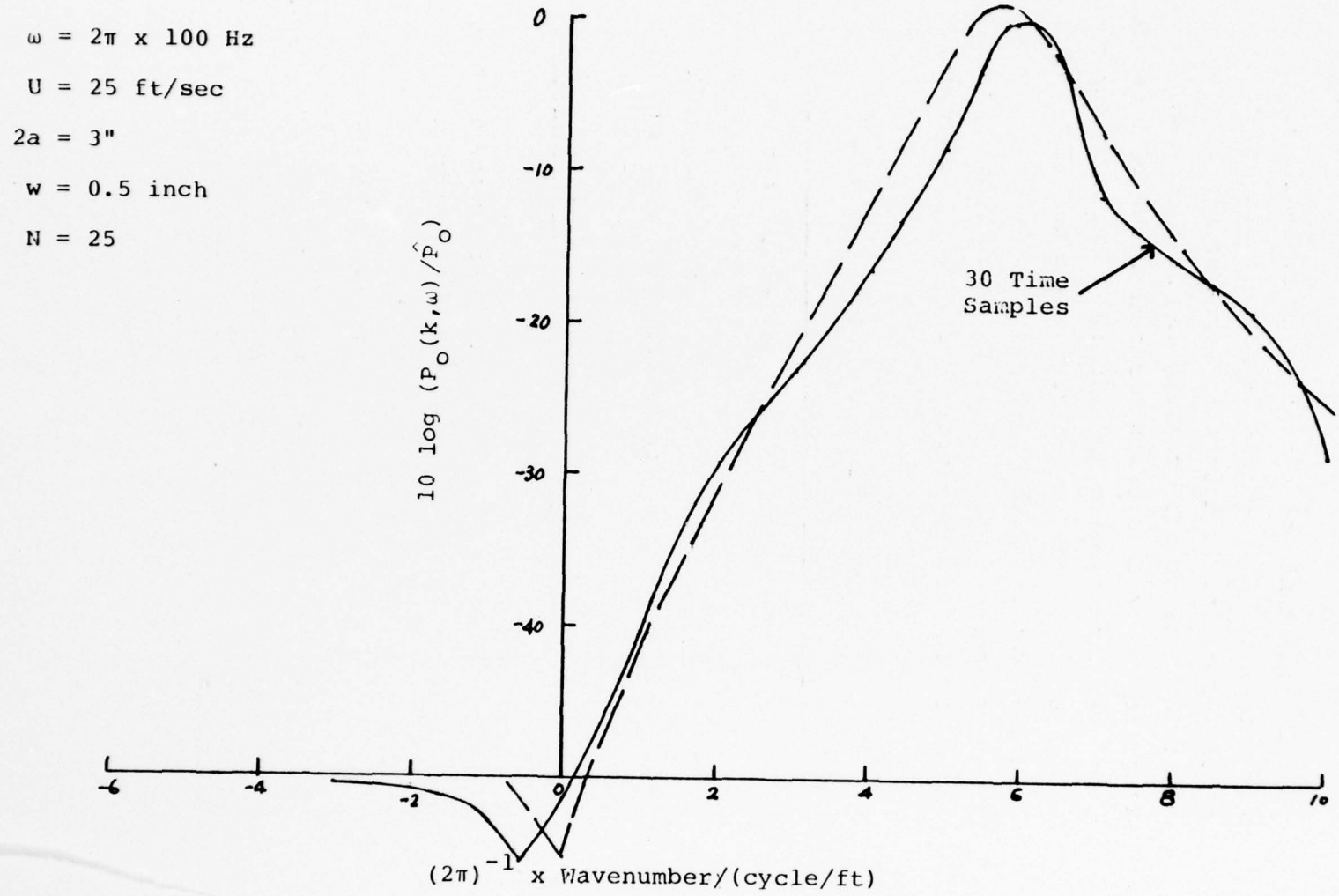

Figure 7. MLE Estimate Using Time Average Correlation Matrix.

6. Summary

In conclusion, we have shown that maximum likelihood wavenumber estimate can be used effectively in the measurement of flow noise. In the presence of sensor error, it is necessary to use a combined technique to estimate the power in different wavenumber regions. With this technique, the acceptable phase error is on the order of 3° (including phase-center placement error, see Eq. (15))and the acceptable amplitude range is between 1 ± 0.06. In computing the correlation matrix for a 25-element array, an average of thirty time samples may be used. Briefly, we summarize the design parameters in Table 2.

Table 2. Measurement Array Design

Number of Elements	25
Element Width	0.5 inch
Element Spacing	0.5 inch
Normalized Amplitude Range	1 ± 0.06
Phase Error	1.5°
Element-Center Error	3 mils

These parameters are probably more stringent than necessary. The analysis on which these figures are based tends to be pessimistic. As compared with the figures given in Reference [1], the tolerances are larger by a factor of 10.

With this design, the measurements should be within 3 dB of the true spectral level everywhere where $k/2\pi$ is above 0.5 cycle/ft. Below this value, the error is larger and, at zero wavenumber, the expected error is about 6 dB.

In designing an array, it is observed that a long array has better resolution and better sidelobe suppression. It is also observed that large gaps between sensor element could cause aliasing error. So, if we are confined to a uniform array, we must increase the number of elements to obtain better performance beyond a certain limit. In Eq. (9), it is clear that the MLE can be applied to arrays with any type of element spacing. As long as the proper steering vector is employed, the best estimate for any configuration can be obtained just as easily as that for a uniform array. Perhaps, with nonuniform spacing, the MLE estimate can be improved without increasing the number of elements. This will be investigated in the future.

References

[1] L.W. Brooks, "Further Results on An Array Design to Measure the Wavenumber-Frequency Spectrum Beneath an Axisymmetric Turbulent Boundary Layer", BSI Report No. CBR-79-01, February 5, 1979.

[2] D.M. Chase, "Modeling of Turbulent Wall-Pressure Spectra on Towed Cylinders", Technical Memo 352, Contract No. N66001-77-C-0114, BBN, May 23, 1977.

[3] S. Gardner, "Summary of Recent Results Concerning Low-Wavenumber Boundary Layer Turbulence", Report 077-106, BSI, January 10, 1977.

[4] J. Capon, "High-Resolution Frequency-Wavenumber Spectrum Analysis", Proceeding of IEEE, August 1969.

[5] R.T. Lacoss, "Data Adaptive Spectral Analysis Methods", Geophysics, August 1971.

Appendix A The Derivatives of the Spectral Estimates, P_L and P_C

From Eqs. (9) and (10), both P_L and P_C are seen to have similar forms. To evaluate the degradation due to sensor errors, the first and second derivatives are derived in this appendix. From Eq. (9), P_L is in the form

$$P_L = Q^{-1} \tag{A-1}$$

where Q is the quadratic form

$$Q = S\ R^{-1} S^{\dagger}$$

$$= \sum_{n,m} b_{nm} s_n s_m^{*} \tag{A-2}$$

and from Eq. (10), P_C has the form

$$N^2\ P_C = Q'$$

$$= S\ R\ S^{\dagger}$$

$$= \sum_{n,m} r_{nm}\ s_n\ s_m^{*} \tag{A-3}$$

The summations are from 1 to N. b_{nm} are certainly different from r_{nm} but both are independent of the variables controlling the steering vectors $\{s_n\}$ which is in the form of

$$s_n = \beta_n \exp(j\theta_n) \tag{A-4}$$

β_n is nominally unity and θ_n depends on the pointing direction.

It will be assumed that the errors are small. Differentiating P_L with respect to θ_ℓ, we obtain from (A-1)

$$\frac{\partial P_L}{\partial \theta_\ell} = -(Q^{-2}) \frac{\partial Q}{\partial \theta_\ell} \tag{A-5}$$

and

$$\frac{\partial^2 P_L}{\partial \theta_\ell} = 2\, Q^{-3} \left(\frac{\partial Q}{\partial \theta_\ell} \right)^2 + (-Q^{-2}) \frac{\partial^2 Q}{\partial \theta_\ell^{\,2}} \tag{A-6}$$

At the same time,

$$N^2 \frac{\partial P_c}{\partial \theta_\ell} = \frac{\partial Q'}{\partial \theta_\ell} \tag{A-7}$$

and

$$N^2 \frac{\partial P_c}{\partial \theta_\ell} = \frac{\partial^2 Q'}{\partial \theta_\ell^{\,2}} \tag{A-8}$$

Since Q and Q' are essentially the same function, we need only to find $\partial^2 Q / \partial \theta_\ell^{\,2}$. We shall hold β_n constant and set them equal to unity. Substituting (A-4) into (A-2) we have

$$Q = \sum_{n,m} b_{nm}\, e^{+j2\pi\theta_n}\, e^{-j2\pi\theta_m} \tag{A-9}$$

and

$$\frac{\partial Q}{\partial \theta_\ell} = \sum_{m \neq \ell} j\, b_{\ell m}\, e^{j\theta_\ell}\, e^{-j\theta_m}$$

$$+ \sum_{m \neq \ell} (-j)\, b_{m\ell}\, e^{j\theta_m}\, e^{-j\theta_\ell} \qquad \text{(A-10)}$$

Since

$$(b_{\ell m}\, e^{j\theta_\ell}\, e^{-j\theta_m})^* = b_{m\ell}\, e^{-j\theta_\ell}\, e^{j\theta_m} \qquad \text{(A-11)}$$

we obtain

$$\frac{\partial Q}{\partial \theta_\ell} = -2 \sum_{m \neq \ell} \mathrm{Im}\,(b_{\ell m}\, e^{j\theta_\ell}\, e^{-j\theta_m}) \qquad \text{(A-12)}$$

where Im(x) is the imaginary part of x. Differentiation of Q a second time with respect to θ_ℓ to obtain $\partial^2 Q/\partial \theta_\ell^2$ yields

$$\frac{\partial^2 Q}{\partial \theta_\ell^2} = \sum_{m \neq \ell} b_{\ell m}\, e^{j\theta_\ell}\, e^{-j\theta_m} - \sum_{m \neq \ell} b_{m\ell}\, e^{j\theta_m}\, e^{-j\theta_\ell}$$

$$= -2 \sum_{k \neq \ell} \mathrm{Re}\,(b_{\ell m}\, e^{j\theta_\ell}\, e^{-j\theta_m}) \qquad \text{(A-13)}$$

where Re(x) is the real part of x. Combining (A-6), (A-12) and (A-13), we obtain the desired result for $\partial^2 P_L / \partial \theta_\ell^{\,2}$. Naturally, if we replace $b_{\ell m}$ in (A-13) by $r_{\ell m}$, we obtain $\partial^2 P_C / \partial \theta_\ell^{\,2}$.

The derivative of P_L and P_C with respect to β_ℓ can be found in a similar way. Eq. (A-6) and (A-8) will hold if $\frac{\partial Q}{\partial \theta_\ell}$ is replaced by $\partial Q / \partial \beta_\ell$. In this case θ_n are held constant. For convenience, in (A-14) to (A-16) they are treated as part of b_{nm} or r_{nm}. Hence,

$$Q = \sum_{n,m} b_{nm}\, \beta_n\, \beta_m \qquad \text{(A-14)}$$

The first derivative of Q is

$$\frac{\partial Q}{\partial \beta_\ell} = 2\, b_{\ell\ell}\, \beta_\ell + \sum_{m \neq \ell} (b_{\ell m}\, \beta_m + b_{m\ell}\, \beta_m)$$

$$= 2 \sum_m \mathrm{Re}\,(b_{\ell m}\, \beta_m) \qquad \text{(A-15)}$$

and the second derivative is simply

$$\frac{\partial^2 Q}{\partial \beta_\ell^{\,2}} = 2\, b_{\ell\ell} \qquad \text{(A-16)}$$

Combining (A-6), (A-15) and (A-16), the desired $\partial P_L^{\,2} / \partial \beta_\ell$ is obtained, i.e.

$$\left. -\frac{\partial P_L^{\,2}}{\partial \beta_\ell^{\,2}} \right|_{\beta_\ell = 1} = 2\, Q^{-3} \left[2 \sum_k \mathrm{Re}\, (b_{\ell m} e^{j\theta_\ell}\, e^{-j\theta_m}) \right]^2 - 2Q^{-2}\, b_{\ell\ell} \qquad \text{(A-17)}$$

and

$$N^2 \left.\frac{\partial P_c^{\,2}}{\partial \beta_\ell^{\,2}}\right|_{\beta_\ell=1} = 2\, b_{\ell\ell} \qquad \text{(A-18)}$$

ONR DISTRIBUTION LIST

	NUMBER OF COPIES
Defense Documentation Center Cameron Station Alexandria, Virginia 22314	12
Director Naval Research Laboratory Code 2627 4555 Overlook Avenue, S.W. Washington, D.C. 20375	6
Office of Naval Research Branch Office 495 Summer Street Boston, Massachusetts 02210	
Office of Naval Research Branch Office 1030 East Green Street Pasadena, California 91106	
Commander Naval Sea Systems Command Department of the Navy Washington, D.C. 20362 Code 06H1	C. Walker
Commander Naval Sea Systems Command Department of the Navy Washington, D.C. 20362 Code 06H2	
Commander Naval Electronic Systems Command Code 320 2511 Jefferson Davis Highway National Center #1 Arlington, Virginia 20360	
Office of Naval Research Branch Office 536 South Clark Street Chicago, Illinois 60605	
Commander Naval Electronic Systems Command PME 124-40 2511 Jefferson Davis Highway National Center #1 Arlington, Virginia 20360	

Commanding Officer
Naval Underwater Systems Center
Central Test & Evaluation Activity
1651 SW 40th Street
Fort Lauderdale, Florida 33315

Commanding Officer
Naval Ocean Research & Development Activity
NSTL Station
Bay St. Louis, Mississippi 39529

Chief of Naval Material
NAVMAT 03T
Arlington, Virginia 20360

Commander
Naval Ocean Systems Center
San Diego, California 92152

Commander
David W. Taylor Naval Ship Research
and Development Center
Bethesda, Maryland 20084

Dr. P. Rispin

C. Campbell
Arthur D. Little, Inc.
Acorn Park
Cambridge, Massachusetts 02140

Binary Systems, Inc.
88 Sunnyside Blvd.
Plainview, New York 11803

Johns Hopkins University
Applied Physics Laboratory
SSBN Security Program
Johns Hopkins Road
Laurel, Maryland 20810

A. M. Chwastyk

EDO Corporation
1310 11th Street
College Point, New York 11356

J. Schere

General Dynamics Corporation
Electric Boat Division
Eastern Point Road
Groton, Connecticut 06340

Project Manager
Anti-Submarine Warfare Systems
Project (PM-4)
Department of the Navy
Washington, D.C. 20362

Capt. R. E. Adler, ASW-13

Office of Naval Research 800 N. Quincy Street Arlington, Virginia 22217	Code 212 H. Fitzpatrick Code 222 G. Boyer
Commander Naval Undersea Center San Diego, California 92132	Dr. R. Smith R. Koelsar
Commanding Officer Naval Underwater Systems Center New London Laboratory New London, Connecticut 06320	Dr. H. Schloemer Dr. W. Strawderman R. Kennedy A. Markowitz E. Racine
Bolt Beranek & Newman, Inc. 50 Moulton Street Cambridge, Massachusetts 02138	Dr. D. Chase Dr. K. Chandiramani
Hughes Aircraft Company Ground Systems Group 1901 West Malvern Avenue Fullerton, California 92634	D. Veronda
Sperry Gyroscope Information and Communication Div. Great Neck, New York 11020	G. Rand
General Electric Company Heavy Military Electronic Systems Syracuse, New York 13201	Don Braite
Raytheon Corporation Submarine Signal Division Portsmouth, Rhode Island 02871	Phil Brooks
Bolt Beranek & Newman, Inc. 1701 North Fort Myer Drive Arlington, Virginia 22209	
Gould Incorporated Chesapeake Instrument Division 6711 Baymeadow Drive Glen Burnie, Maryland 21061	
Professor Patrick Leehey Room 5-222 Massachusetts Institute of Technology Acoustics and Vibration Laboratory 70 Massachusetts Avenue Cambridge, Massachusetts 02139	

Professor W. W. Willmarth
The University of Michigan
Aerospace Engineering, North Campus
Ann Arbor, Michigan 48109

Binary Systems, Inc.
10750 Columbia Pike
Silver Spring, Maryland 20901

F. Rees

MAR, Inc.
1335 Rockville Pike
Rockville, Maryland 20852

REPORT DOCUMENTATION PAGE

READ INSTRUCTIONS BEFORE COMPLETING FORM

1. REPORT NUMBER (14) WBR-79-2	2. GOVT ACCESSION NO.
3. RECIPIENT'S CATALOG NUMBER	
4. TITLE (and Subtitle) (6) Wavenumber Spectral Measurement of Turbulent Boundary Layer Wall Pressure by Maximum Likelihood Methods.	5. TYPE OF REPORT & PERIOD COVERED (9) Final rept.
	6. PERFORMING ORG. REPORT NUMBER
7. AUTHOR(s) (10) Dr. P. S. Tong	8. CONTRACT OR GRANT NUMBER(s) (15) ONR - N00014-72-C-0318
9. PERFORMING ORGANIZATION NAME AND ADDRESS Binary Systems, Inc. 10750 Columbia Pike Silver Spring, Maryland 20901	10. PROGRAM ELEMENT PROJECT, TASK AREA & WORK UNIT NUMBERS
11. CONTROLLING OFFICE NAME AND ADDRESS Office of Naval Research, Code 222 800 N. Quincy Street Arlington, Virginia 22217	12. REPORT DATE (11) Apr[illegible]79 13. NUMBER OF PAGES 43
14. MONITORING AGENCY NAME & ADDRESS (if different from Controlling Office) N/A (12) 44	15. SECURITY CLASS. (of this report) Unclassified 15a. DECLASSIFICATION/DOWNGRADING SCHEDULE

16. DISTRIBUTION STATEMENT (of this Report)

Unlimited

17. DISTRIBUTION STATEMENT (of the abstract entered in Block 20, if different from Report)

18. SUPPLEMENTARY NOTES

19. KEY WORDS (Continue on reverse side if necessary and identify by block number)

TURBULENT BOUNDARY LAYER PRESSURE FLUCTUATION
MAXIMUM LIKELIHOOD SPECTRAL ANALYSIS
LOW WAVENUMBER SPECTRUM
WAVE VECTOR FILTERING

20. ABSTRACT (Continue on reverse side if necessary and identify by block number)

A combined procedure based on conventional and maximum likelihood spectral estimation techniques is proposed for the measurement of turbulent boundary layer pressure fluctuation wavenumber spectrum. It is shown that the mixed procedure is more tolerant to sensor inaccuracies in amplitude, phase or phase center alignment.

DD FORM 1 JAN 73 1473 EDITION OF 1 NOV 65 IS OBSOLETE
S/N 0102-LF-014-6601

SECURITY CLASSIFICATION OF THIS PAGE (When Data Entered)

410 409